

Optical Engineering

OpticalEngineering.SPIEDigitalLibrary.org

Image quality, meteorological optical range, and fog particulate number evaluation using the Sandia National Laboratories fog chamber

Gabriel C. Birch
Bryana L. Woo
Andres L. Sanchez
Haley Knapp

SPIE.

Gabriel C. Birch, Bryana L. Woo, Andres L. Sanchez, Haley Knapp, "Image quality, meteorological optical range, and fog particulate number evaluation using the Sandia National Laboratories fog chamber," *Opt. Eng.* **56**(8), 085104 (2017), doi: 10.1117/1.OE.56.8.085104.

Image quality, meteorological optical range, and fog particulate number evaluation using the Sandia National Laboratories fog chamber

Gabriel C. Birch,* Bryana L. Woo, Andres L. Sanchez, and Haley Knapp

Sandia National Laboratories, Albuquerque, New Mexico, United States

Abstract. The evaluation of optical system performance in fog conditions typically requires field testing. This can be challenging due to the unpredictable nature of fog generation and the temporal and spatial nonuniformity of the phenomenon itself. We describe the Sandia National Laboratories fog chamber, a new test facility that enables the repeatable generation of fog within a $55\text{ m} \times 3\text{ m} \times 3\text{ m}$ ($L \times W \times H$) environment, and demonstrate the fog chamber through a series of optical tests. These tests are performed to evaluate system image quality, determine meteorological optical range (MOR), and measure the number of particles in the atmosphere. Relationships between typical optical quality metrics, MOR values, and total number of fog particles are described using the data obtained from the fog chamber and repeated over a series of three tests. © The Authors. Published by SPIE under a Creative Commons Attribution 3.0 Unported License. Distribution or reproduction of this work in whole or in part requires full attribution of the original publication, including its DOI. [DOI: [10.1117/1.OE.56.8.085104](https://doi.org/10.1117/1.OE.56.8.085104)]

Keywords: fog; image quality; optical testing.

Paper 170385 received Mar. 16, 2017; accepted for publication Aug. 1, 2017; published online Aug. 24, 2017.

1 Introduction

Reduced visibility due to the presence of fog can significantly impact the performance of an imaging system. Understanding these performance degradations affects many diverse areas of engineering, from aviation to physical security. We report on a newly developed fog generation test facility and optical testing performed within this facility. Constructed at Sandia National Laboratories, the fog generation facility consists of a $55\text{ m} \times 3\text{ m} \times 3\text{ m}$ chamber capable of generating fog conditions through the spraying of water mixed with user-specified seeding chemicals.

In this study, we utilize NaCl seeded water mixtures to evaluate imaging system performance in a simulated coastal fog. We report on measurements of relative spatial frequency response (SFR) area under curve (AUC), meteorological optical range (MOR), and total number of fog particles present within the test chamber. All values are measured in 1-s temporal periods. A commercial security camera was used to record imagery throughout testing, in conjunction with a Malvern Spraytec Particle Sizer Instrument used to measure the number of fog particles in the test chamber.

This document begins by discussing past simulations, tests, and test facilities used to examine the impact of fog on optical system performance. A description of the Sandia fog chamber, as well as details regarding instrumentation used to measure fog particle size distribution, is provided. The MOR metric is discussed, and detail regarding the utilization of a sinusoidal Siemens star test target to measure imaging system SFR is included. Three fog chamber tests at varying distances and fog densities are discussed. Relationships between the relative SFR AUC, MOR, and fog particle number quantities are found to follow expected behavior; however, relative SFR AUC was found to recover much faster

than would be expected based on MOR measurements while the fog was dissipating.

2 Background

Dispersive media's effect on light propagation poses distinct challenges in many fields. Several studies focus on light propagation through obscurants and its effect on automobile safety, optical communication, and the modulation transfer function of optical systems.¹⁻⁶ Other studies have examined the effect of wavelength on light penetration through dispersive media.⁷⁻⁹ Simulations have been utilized to examine foundational aspects of photon propagation through scattering media,¹⁰⁻¹⁴ but these studies often assume model parameters such as monodispersed droplet size and homogeneous atmospheric conditions.^{1,15}

Validating models and measuring performance degradations typically involve field testing within naturally occurring fog.^{1,6} However, evaluating system performance through field testing can prove challenging due to the temporally unpredictable behavior of naturally occurring environmental conditions such as fog.¹⁶ In the instances where natural fog occurs in the appropriate density for the desired test, it is difficult to collect composition data such as uniformity or number and size of particles, especially at multiple points along a testing path. The dissipation of the fog may also result in incomplete or inconsistent data with which to compare. Alternatively, the physical testing for fog can be implemented in controlled laboratory environments^{17,18} through the creation of fog chambers.

An early fog chamber was created by Houghton¹⁹ in 1931 using wooden containers of $0.3\text{ m} \times 0.025\text{ m} \times 0.025\text{ m}$ with detectors and light sources at either end. This early fog chamber experienced many of the challenges present in natural fog testing, including instability and rapid particulate dissipation, and made exact fog densities difficult to replicate due to dependence on the surrounding atmosphere.¹⁹ Recent fog

*Address all correspondence to: Gabriel C. Birch, E-mail: gobirch@sandia.gov

chambers include the 22 m × 2.4 m × 2.4 m Defense R&D Canada fog chamber. This chamber uses a series of six fans located on the floor to distribute particulates and permits users to simulate scattering environments with materials such as water, talcum powder, and Dualite MS3 powder. Located outdoors, the chamber has entrances on either end that open to expose the fog or dust for testing. A Malvern Spraytec particle size analyzer is used for monitoring the fog concentration and droplet size within this facility.¹⁸

An additional fog generation and testing facility was created by the Federal Aviation Administration using a 249.9 m × 9.14 m × 3.04 to 9.14 m indoor glide facility, located at the University of California, Berkeley. The chamber was divided into 24 sections and allowed for different densities of fog in each section. The fog was created by atomizing water as it moved through an air pressurized nozzle.²⁰ This chamber, however, does not appear to be in use.² A more recent fog chamber was built by the European Union (EU) in France to allow public industry a place to test equipment in fog conditions. The EU fog chamber is 30 m × 5.5 m × 2 m and located outdoors, similar to the Defense R&D Canada chamber. Desired visibility is reached by filling the chamber to a very dense fog then allowing natural dissipation to occur until the appropriate visibility level is reached. In order to stabilize the fog at the desired density, small bursts of water are added to the chamber to compensate for particulate evaporation and fall out. The stabilization process applied to the EU chamber allows a consistent, dense fog to be maintained regardless of outside conditions. Though the dense fog is able to be stabilized, light fog still dissipates quickly. This chamber is primarily used for testing automotive lights and street sign visibility in fog.² Other smaller fog chambers have been created, including the electro-optical test facility fog chamber²¹ and the VALEO Bobigny fog chamber.¹⁷

Along with these fog generation facilities, there are chambers designed for the production of clouds. The 30-m³, high-flow turbulent cloud chamber, located in the Netherlands, has the ability to make stable, reproducible clouds that can last for hours. The cloud is formed by supersaturating the atmosphere using a humidifier and then creating a temperature difference between two areas. This chamber is primarily used to evaluate how pollutants in the air affect rain formation from clouds. Seeding the air with ammonium sulfate and sodium sulfate causes the water droplets to form around the molecules giving the cloud different physical and chemical properties than a pure water seed.²²

These fog generation and testing facilities provide unique capabilities relevant to their primary scientific utilization. However, the available capabilities of these chambers do not overlap and leave capabilities to be desired. The Sandia National Laboratories fog generation test facility (SNL fog chamber) was designed with four key differentiating factors in mind. First, the SNL fog chamber provides a significant size increase compared to currently used fog chambers with an added length of 25 m over the largest reported chamber. Second, the facility is temperature controlled and allows the fog environment to be maintained for extended periods. Testing equipment can be placed directly in the fog chamber with the operator outside to prevent the need to expose the fog after generation. Third, the fog chamber can use seeded fog. This fog, as discussed previously, provides

different physical and chemical properties compared to standard water fog. The seeds allowed for the generation of salt-seeded coastal fog for the tests implemented in the remainder of this document. Finally, a Malvern Spraytec particle size analyzer is used in the facility to monitor fog particle size and distribution. In the remainder of this work, we demonstrate this fog generation facility by evaluating visible imager performance and fog particulate values over time.

3 Methodology

A testing facility and method used to evaluate visible imager performance is described. Specific attributes of the Sandia National Laboratories fog chamber, as well as techniques used to collect particle size distribution data are included in Sec. 3.1. Proof-of-concept tests were performed to evaluate the fog chamber using a visible band imager. Responses of SFR AUC and MOR to variations of fog density were the performance criteria used in these tests. Section 3.2 describes how MOR degradations were measured. Section 3.3 describes the utilization of a sinusoidal Siemens star test target to measure relative SFR AUC. Finally, the proof-of-concept tests are described in Sec. 3.4.

3.1 Fog Generation Test Facility

The Sandia National Laboratories (SNL) fog chamber, shown in Fig. 1, is ~55 m × 3 m × 3 m ($L \times W \times H$). The test facility purpose is primarily to test and evaluate optical systems, such as visible cameras, thermal imagers, or laser-based devices, within a stable laboratory environment. The SNL fog chamber has the capability of utilizing differing chemical constituents to seed the fog mixture with environmentally relevant products using 64 two-fluid air-atomizing nozzles. In this proof-of-concept test, the simulated fog was seeded with a 10 g/LNaCl salt water mixture. NaCl was chosen to closely mimic the primary constituent found in naturally forming sea coastal fog.^{23–25} The chamber is separated into three sections, which enable varying fog densities and particulate concentrations. However, for the purposes of test consistency, all sections were run with the same nozzle conditions: an air flow rate of 3 to 4 cubic feet per minute and a liquid flow rate of 115 mL/min.

Particle size distribution is measured in 1-s intervals using a Malvern Spraytec instrument and inhalation cell accessory. The Malvern Spraytec instrument calculates particle size, which is inversely proportional to scattering angle, via indirect measurements of light scatter off particulates onto a detector. Mie theory, which predicts absorption and light scatter intensity of a spherical particle, is the fundamental model that the Malvern software utilizes to determine particle size.^{24,26,27} Additionally, the inhalation cell accessory was used as an enclosed measurement zone with a controlled sample flow rate. This is important for particle size accuracy and postmeasurement concentration calculations, which utilizes the Beer–Lambert law and particle diameter to determine volume concentration. Accuracy of the particle size measurements was verified using the wet dispersion cell accessory and NIST traceable standards. Verification was determined by the manufacturer by taking measurements of three different polystyrene latex sphere sizes at 1, 9, and 40 μm. The Malvern instrument correctly predicted test particle size to within ±1% accuracy.

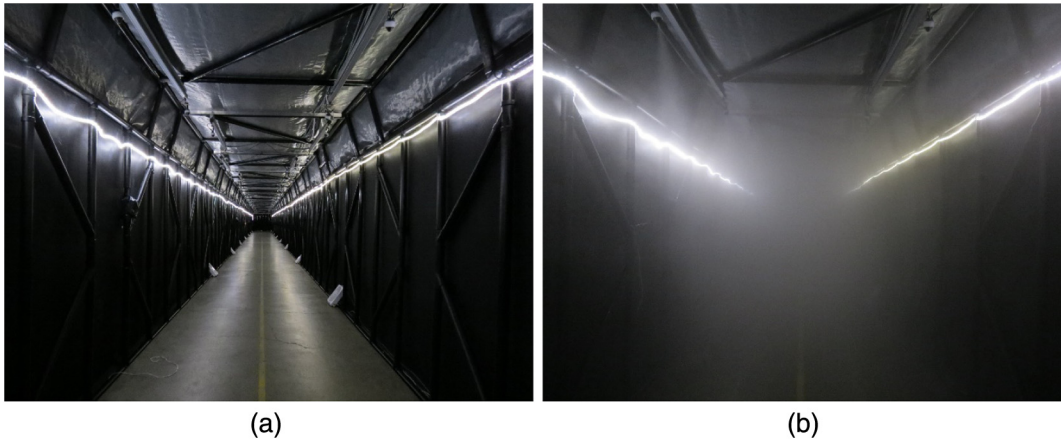


Fig. 1 (a) SNL fog chamber under nominal conditions and (b) SNL fog chamber with simulated coastal fog. Safety LED lights were kept on in these images to demonstrate the scattering nature of the generated fog. However, subsequent tests removed all sources of illumination except for the test source located within the test target chamber.

During data collection, the Malvern Spraytec calculates particle size measurements as volume-based results. Restated, each particle size bin consists of a derived percentage of the total volume of all particles in the distribution. These data are then converted to a number-based (i.e., number per cubic centimeter) distribution by²⁴

$$n_N(D_p) = \frac{6n_V(D_p)}{\pi D_p^3}, \quad (1)$$

where D_p is the particle diameter in micrometers and n_V is the volume-based distribution, which is equal to

$$n_V(D_p) = V_F \times V_T, \quad (2)$$

where V_T is the total volume concentration in parts per million (i.e., ratio of total volume of particles to total volume of air sampled) and V_F is the volume fraction (i.e., percent volume) of all particles within a particular size range in the total size distribution.

3.2 Meteorological Optical Range Calculations

Metrics defining the transparency of the atmosphere are utilized in several domains such as aviation, meteorology, transportation, and shipping. The prominent metric was once termed “visual range” but has since become known as visibility.²⁸ Classically, visibility was a quantity that was determined subjectively by an observer. However, an alternative visibility metric exists today that is quantitatively defined as the distance required to reduce the luminous flux of a collimated beam from a 2700-K color temperature lamp to 5% of its original value. This metric is known as the MOR. For the tests performed in this study, we utilize an MOR measurement to provide quantitative and repeatable measurements of the optical effects of fog on visible imager performance. The concepts of the MOR are founded on the Beer–Lambert law,²⁹ which states that

$$I = I_0 e^{-\alpha d}, \quad (3)$$

where I is the intensity of the measured target, I_0 is the nominal intensity, α is the attenuation coefficient, and d is the

distance at which the source is located from the detector. Solving for α yields

$$\alpha = \frac{\ln\left(\frac{I}{I_0}\right)}{-d}. \quad (4)$$

To calculate MOR, we define the ratio of the measured intensity to the nominal intensity as 5%. Mathematically, we define this as follows:

$$\frac{I}{I_0} = 0.05 = e^{-\alpha d_{\text{MOR}}}. \quad (5)$$

Inserting Eq. (4) into Eq. (5) and solving for d yields the MOR (i.e., the distance at which intensity reduces to 5%)

$$d_{\text{MOR}} = d \times \frac{\ln(0.05)}{\ln\left(\frac{I}{I_0}\right)}. \quad (6)$$

MOR measurements were implemented with a short baseline transmissometer configuration created using a white light emitting diode (LED) as the emitter and a standard camera sensor as the photodetector. While not strictly conforming to the collimation and 2700-K color temperature of the source, this configuration enables simple evaluation of optical degradations caused by scattering particulates using an unchanging source and sensor pair. Pixels within a known white and black target region of an optical test target were averaged to obtain intensity measurements. Initial measurements were obtained without fog present in the fog chamber and used as the nominal intensity value. Knowledge of the target distance, I , and I_0 values enables the calculation of a relative MOR measurement compared to nominal, pefog conditions. As short baseline transmissometers are most accurate in the 4- to 128-m range, all tests were implemented within these shorter distances.³⁰

3.3 Relative Spatial Frequency Response Area under Curve Methods

Measurement of SFR can be achieved via a number of methods.³¹ We chose to utilize a sinusoidal Siemens star test target as described by the ISO 12233 photography resolution standard. Motivation to utilize the sinusoidal Siemens star test rather than the more common slanted edge measurement

is due to the presence of algorithmic edge enhancements applied to captured images from the camera tested. These edge enhancements artificially alter the contrast recorded by the camera at the slanted edge and thus modify the SFR if slanted edge techniques are utilized. Previous work suggests that the sinusoidal Siemens star test is less sensitive to artifacts induced by edge enhancement algorithms.³²

However, the use of a sinusoidal Siemens star target can be complicated due to incorrect determinations of the test target center. Care must be taken to precisely identify the center of the test target either using closed form mathematics for curve fitting of decentered radial sinusoid profiles or increasing the number of radial segments used to fit a sine wave to measured data.³³ In this analysis, we utilized 64 sinusoidal Siemens star segments to mitigate errors due to misidentified target centers.

SFR AUC nominal measurements were taken before fog generation began. All subsequent SFR data were then normalized by the nominal set, and a trapezoidal numerical integration was performed to find the SFR AUC for every 1-s interval during a test. This method of normalization was used to account for imperfections in the imaging system or residual defocus that reduced the absolute SFR of the system at the beginning of a test, enabling direct measurement of the impact of atmospheric conditions on optical performance.

3.4 Proof of Concept Test Method

A Lumenera Li165 color network surveillance camera was used to evaluate the effects of fog density on reported relative

SFR AUC and MOR for different fog levels in the SNL fog chamber facility. The camera was placed in a weatherproof casing and mounted on a tripod at the end of the fog tunnel. An open test target chamber with positive pressure housed an optical test target consisting of sinusoidal Siemens star targets and grayscale patches conforming to the ISO 12233 standard. The test target chamber contained two LED illumination sources oriented toward the test target. These light sources were the only illumination within the testing facility during the duration of a test. The camera was focused by visually maximizing the aliasing of the high-frequency elements of the sinusoidal Siemens star test target before fog was generated. Video was then recorded from the camera for the duration of a test, and frames were averaged together into 1-s intervals to match that of the Malvern Spraytech system. These 1-s interval datasets were then utilized to calculate relative SFR AUC and MOR, as previously described.

Figure 2(a) shows a diagram of the test setup, whereas Figs. 2(b)–2(d) show images of the test target captured by the camera with increasingly dense fog.

Nominal measurements were recorded from the camera for the duration of 1 min prior to fog generation. The camera was allowed to continue recording during the course of fog generation while concurrent particle number measurements were collected by the Malvern Spraytec instrument. Fog generation continued until fog density was so great that the test target became visually obscured. At this point, fog generation was stopped and natural dissipation of fog particles occurred.

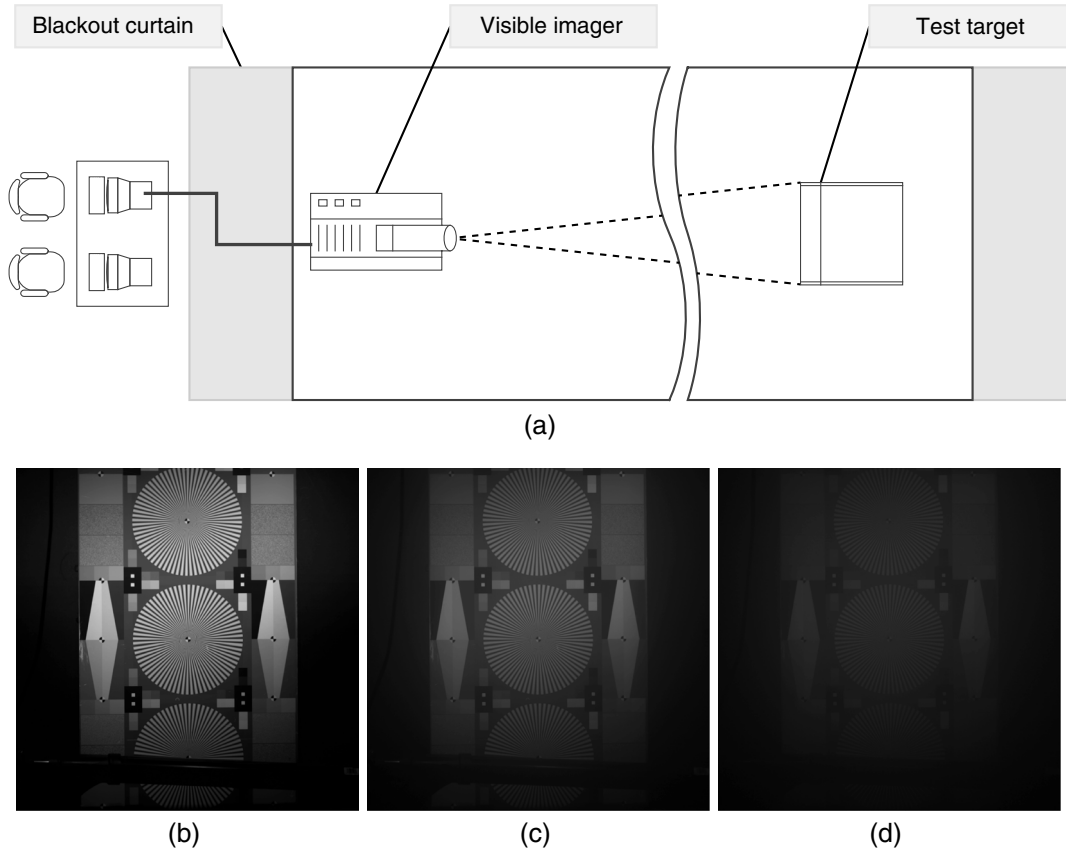


Fig. 2 (a) Diagram of the SNL fog chamber and test configuration used in this study and (b)–(d) images captured by the Li165 camera with increasing fog density.

This test procedure was repeated three times for test targets located at 10, 20, and 30 feet from the camera.

4 Results

4.1 Test One

Test one placed the optical test target ~10 feet from the camera. Fog generation proceeded for ~20 min, until test target visibility was almost completely reduced, whereupon fog generation was halted. Fog dissipation began to reduce the total number of particles in the chamber.

Figure 3(a) shows the recorded values of relative SFR AUC, Fig. 3(b) shows MOR, and Fig. 3(c) shows the total number of particles in the atmosphere as measured by the Malvern Spraytec instrument. All values are a function of time, discretized into 1-s averages as described in the test methodology section.

Relative SFR AUC quickly decreased with the initial generation of fog particles, until a minimum value was reached within the 665- to 1340-s period. Once fog generation was stopped, relative SFR AUC rapidly increased for ~300 s, followed by a slower increase in relative SFR AUC for the remainder of the test.

Similarly, MOR rapidly decreased until a minimum value of ~17 feet was achieved between 500 and 1375 s. After fog generation was stopped, MOR began a uniform and nearly linear increase for the remainder of the test.

The total number of particles increased during fog generation. The average particle size distribution with a volume-based concentration was bimodal with peaks at 4.6 and 34 μm . However, when converted to a number-based distribution, the peak particle size was 1.4 μm . This indicates that, while large particles are present in the chamber, the majority of particles were small (i.e., <10 μm). Once fog generation stopped, particles naturally fell out of the atmosphere due to gravitational settling and evaporation affects which, reduced the total number of particles over time. During fall out, the larger particles fall out of air faster than the smaller particles, resulting in a nonlinear decay in the number of particles present within the chamber.

4.2 Test Two

Test two increased the distance to the optical test target, placing the target ~20 feet from the camera. Figures 4(a)–4(c) show test results. Due to the increased atmospheric column, a lower fog density was capable of reducing the measured MOR to its minimum point. Fog generation proceeded for ~260 s. After fog generation halted, a decay in the total number of particles occurred for the duration of the test, similar to that shown in Fig. 3(c).

A similar rapid recovery of relative SFR AUC began at ~450 s, followed by a period of slower recovery starting at 870 s. This test produced elevated relative SFR AUC measurements within time periods of MOR measurements less than the test distance. This spurious increased SFR AUC

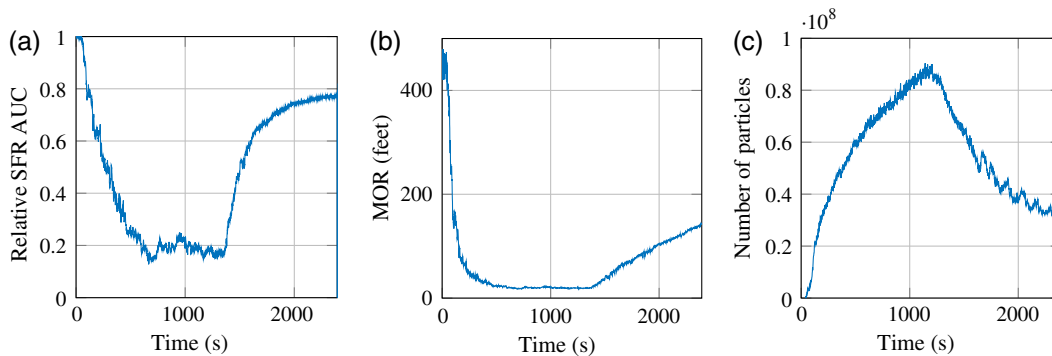


Fig. 3 (a) Relative SFR AUC, (b) MOR, and (c) total number of particles in the atmosphere during test one. All data are plotted versus time in seconds. This test located the optical test target 10 feet from the camera.

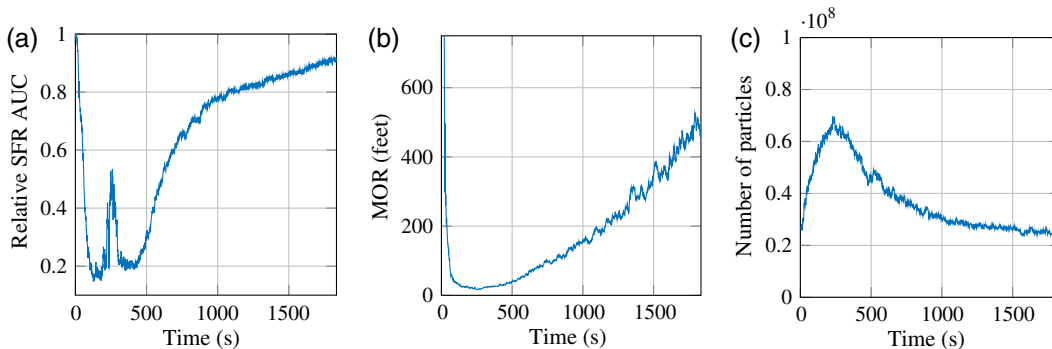


Fig. 4 (a) Relative SFR AUC, (b) MOR, and (c) total number of particles in the atmosphere during test two. All data are plotted versus time in seconds. This test located the optical test target 20 feet from the camera.

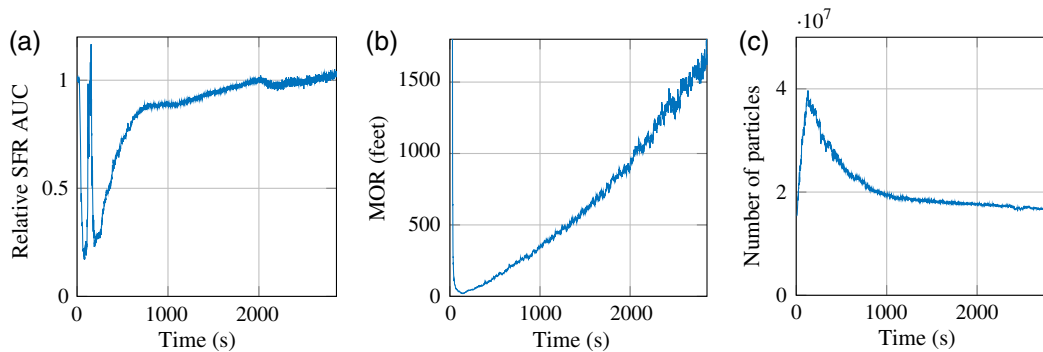


Fig. 5 (a) Relative SFR AUC, (b) MOR, and (c) total number of particles in the atmosphere during test three. All data are plotted versus time in seconds. This test located the optical test target 30 feet from the camera.

occurs due to the sinusoidal Siemens star algorithm. This algorithm takes best-fit amplitude and divides by signal DC offset to retrieve a contrast metric at a specific spatial frequency.³¹ The fog environment scatters spatial information and thus causes best-fit amplitude to decrease rapidly to a near-constant noise value. However, it is still possible for DC offset to change after the sinusoidal best-fit amplitude has reached this near-constant noise value. As fog density increases, and thus DC offset of sinusoidal signals from the imager decreases, a spurious increase in relative SFR AUC occurs.

MOR quickly decreased to values smaller than 20 feet. This would imply that less than 5% of the original intensity was being measured by the imager during the thickest fog. After fog generation was halted, MOR recovered similar to Fig. 3(b).

4.3 Test Three

Test three placed the optical test target ~ 30 feet from the camera. Similar behavior to both test one and test two was shown, with a lower particle density needed to reduce MOR due to comparatively larger optical path length. Test results are shown in Fig. 5. MOR rapidly declined to less than the test target distance and increased near-linearly after fog generation was halted. The spurious relative SFR AUC region increased in value during times when MOR was extremely low, but it showed a similar relative SFR AUC recovery after fog generation stopped, followed by a period of slower relative SFR AUC recovery for the duration of the test.

4.4 Discussion

Results obtained in tests one through three show generally similar behavior for the number of particles versus time. A lower fog density was needed to reduce system performance as the target distance increased, and particulate decay after fog generation was halted proceeded in a similar manner for each test. MOR measurements across each test showed a similar rapid decay as fog generation began, followed by a nearly linear increase in MOR after fog generation was halted. However, relative SFR AUC exhibited unexpected behavior; each test demonstrated a period of rapid relative SFR AUC recovery, followed by a slower recovery of relative SFR AUC. We hypothesize that the relative SFR AUC metric is more susceptible to the presence of large particulates; large particulates more rapidly fall out of

the atmosphere due to gravitational settling when fog generation is suspended, causing the initial rapid recovery of relative SFR AUC.

5 Summary and Future Work

The Sandia National Laboratories fog chamber was demonstrated in a set of tests evaluating relative SFR AUC, MOR, and number of particles in the chamber. Three tests were implemented within the test chamber at varying distances. Each test consisted of an optical test target placed within the fog chamber and illuminated by two white light LEDs. Data were obtained for each distance without fog. The chamber was then filled with fog until the test target was completely obscured. Fog generation was halted, and dissipation was allowed to occur. Imagery data and particle size data were measured during the entire period of fog generation and dissipation. Relationships between the MOR and fog particle number followed the general expected pattern in obscurants. However, relative SFR AUC was found to recover much faster than would be expected based on MOR measurements. It is hypothesized that this initial period of increased recovery rate is due to rapid large particle fall out at the beginning of fog dissipation.

Future work will investigate relative SFR AUC, MOR, and number of particles in the atmosphere using different imaging systems. In particular, quantitative performance metrics in the long wave infrared (LWIR) are of interest to evaluate visible versus LWIR trade-offs in physical security systems. Additional work will investigate more complex constituents including chemical blends that mimic fog, smog, or haze caused by pollutants.

Acknowledgments

Sandia National Laboratories is a multimission laboratory managed and operated by the National Technology and Engineering Solutions of Sandia, LLC, a wholly owned subsidiary of Honeywell International, Inc., for the U.S. Department of Energy's National Nuclear Security Administration under contract No. DE-NA0003525. SAND2017-0636 J.

References

1. E. Dumont, N. Hautiere, and R. Gallen, "A semi-analytic model of fog effects on vision," in *Atmospheric Turbulence, Meteorological Modeling and Aerodynamics*, Nova Science Publishers, Hauppauge, New York (2010).

2. M. Colomb et al., "An innovative artificial fog production device improved in the european project 'fog,'" *Atmos. Res.* **87**(34), 242–251 (2008).
3. H. Manor and S. Arnon, "Performance of an optical wireless communication system as a function of wavelength," *Appl. Opt.* **42**, 4285–4294 (2003).
4. J. Zeller and T. Manzur, "Effect of atmosphere on free-space optical communication networks for border patrol," *Proc. SPIE* **7666**, 766609 (2010).
5. B. R. Strickland et al., "Effects of fog on the bit-error rate of a free-space laser communication system," *Appl. Opt.* **38**, 424–431 (1999).
6. L. R. Bissonnette, "Imaging through fog and rain," *Opt. Eng.* **31**(5), 1045–1052 (1992).
7. J. H. Taylor and H. W. Yates, "Atmospheric transmission in the infrared," *J. Opt. Soc. Am.* **47**, 223–226 (1957).
8. M. R. Clay and A. P. Lenham, "Transmission of electromagnetic radiation in fogs in the 0.53–10.1- μm wavelength range," *Appl. Opt.* **20**, 3831–3832 (1981).
9. D. G. Crowe, D. K. Cohen, and E. L. Dereniak, "Infrared propagation and performance modeling at the electro-optical test facility," *Appl. Opt.* **19**, 1953–1958 (1980).
10. J. C. Ramella-Roman, S. A. Prael, and S. L. Jacques, "Three Monte Carlo programs of polarized light transport into scattering media: part II," *Opt. Express* **13**, 10392–10405 (2005).
11. M. Grabner and V. Kvicera, "Multiple scattering in rain and fog on free-space optical links," *J. Lightwave Technol.* **32**, 513–520 (2014).
12. J. D. van der Laan et al., "Variation of linear and circular polarization persistence for changing field of view and collection area in a forward scattering environment," *Proc. SPIE* **9853**, 98530L (2016).
13. J. D. van der Laan et al., "Range and contrast imaging improvements using circularly polarized light in scattering environments," *Proc. SPIE* **8706**, 87060R (2013).
14. J. Han et al., "Resolution enhancement in active underwater polarization imaging with modulation transfer function analysis," *Appl. Opt.* **54**, 3294–3302 (2015).
15. B. Ben-Dor et al., "Cloud, fog, and aerosol effect on the MTF of optical systems," *Proc. SPIE* **2580**, 106–114 (1995).
16. I. Gultepe et al., "Fog research: a review of past achievements and future perspectives," *Pure Appl. Geophys.* **164**(6), 1121–1159 (2007).
17. E. Belin et al., "Display of an analytical model for backscattered luminance and a full-field range gated imaging system for vision in fog," *Proc. SPIE* **7088**, 70880O (2008).
18. V. Larochelle et al., "Performance assessment of various imaging sensors in fog," *Proc. SPIE* **3364**, 66–80 (1998).
19. H. G. Houghton, "The transmission of visible light through fog," *Phys. Rev.* **38**, 152–158 (1931).
20. J. Ruden et al., "Motorists requirements for active grade crossing warning devices," Technical Report, US Department of Transportation Federal Highway Administration, Traffic Systems Division, Washington, DC (1977).
21. D. K. Cohen, J. H. Hunt, and D. G. Crowe, "Characteristics of a chamber used for electrooptical device performance measurements in the presence of fog," *Appl. Opt.* **21**, 2399–2404 (1982).
22. A. Khlystov, G. Kos, and H. T. Brink, "A high-flow turbulent cloud chamber," *Aerosol Sci. Technol.* **24**, 59–68 (1996).
23. R. Gieray et al., "Phase partitioning of aerosol constituents in cloud based on single-particle and bulk analysis," *Atmos. Environ.* **31**(16), 2491–2502 (1997).
24. J. Seinfeld and S. Pandis, *Atmospheric Chemistry and Physics: From Air Pollution to Climate Change*, Wiley, Hoboken, New Jersey (2016).
25. S. J. Duffy et al., *Environmental Chemistry: A Global Perspective*, Oxford University Press Inc., New York City, New York (2011).
26. W. C. Hinds, *Aerosol Technology: Properties, Behavior, and Measurement of Airborne Particles*, John Wiley & Sons, Hoboken, New Jersey (2012).
27. H. C. Van de Hulst and V. Twersky, "Light scattering by small particles," *Phys. Today* **10**(12), 28–30 (1957).
28. W. K. Middleton, *Vision Through the Atmosphere in Geophysik II/Geophysics II*, Springer, New York City, New York (1957).
29. World Meteorological Organization, "Guide to meteorological instruments and methods of observation," in *Book Guide to Meteorological Instruments and Methods of Observation*, Wallingford, Oxon (2006).
30. D. Griggs et al., "The first WMO intercomparison of visibility measurements, United Kingdom 1988/1889," Final Report WMO/TD (401), Geneva, Switzerland (1990).
31. International Organization for Standardization, Technical Committee Photography, "ISO-12233:2017-photography: electronic still-picture cameras-resolution measurements," 3rd ed., <https://www.iso.org/standard/71696.html> (January 2017).
32. C. Loeblich et al., "Digital camera resolution measurement using sinusoidal Siemens stars," *Proc. SPIE* **6502**, 65020N (2007).
33. G. C. Birch and J. C. Griffin, "Sinusoidal Siemens star spatial frequency response measurement errors due to misidentified target centers," *Opt. Eng.* **54**(7), 074104 (2015).

Gabriel C. Birch received his PhD in optical sciences from the University of Arizona, College of Optical Sciences, in 2012. He is a scientist at Sandia National Laboratories. His current research interests include physical security systems, testing and evaluation of imaging devices, and nontraditional imaging systems.

Bryana L. Woo received her BS and MS degrees in electrical engineering from the New Mexico Institute of Mining and Technology. She is an electronics engineer at Sandia National Laboratories. Her work at Sandia National Laboratories has included modeling plasma physics, evaluating imaging systems, investigation of novel imaging devices, and implementing physical security systems.

Andres L. Sanchez received his MS degree in chemical engineering from the University of New Mexico in 2012. He is a scientist at Sandia National Laboratories. His current research includes atmospheric science and aerosol characterization, as well as chemical and biological dissemination and decontamination.

Haley Knapp is a student in optical engineering at the University of Rochester. She was an optical scientist at Sandia National Laboratories in 2016. She is currently an optical engineer specializing in optomechanics and stray light analysis at Ball Aerospace Technologies.